Anisotropic Subsurface Scattering Acquisition Through a Light Field Based Apparatus

Yurii Piadyk, Yitzchak Lockerman and Claudio Silva; New York University, NY, USA

Abstract

Subsurface scattering gives a distinct look to many everyday objects. However, until now, systems to acquire subsurface scattering have assumed that the subsurface displacement and angle of scattering are completely independent of the angle of incident. While this independence substantially simplifies the acquisition and rendering of materials where it holds true, it makes the acquisition of other materials impossible. In this paper, we demonstrate a system that can quickly acquire the full anisotropic subsurface scattering at a given point. Unlike many existing commercial acquisition systems, our system can be assembled from off-the-shelf optical component and 3D printed/cut parts, making it accessible at a low price. We validate our device by measuring and fitting a dipole model for material exhibiting isotropic subsurface scattering as well as comparing real-world appearance with rendering of anisotropic material under incident laser beam illumination.

Introduction

Many physical objects exhibit subsurface scattering leading to distinctive appearances. In computer graphics, subsurface scattering is modeled by the Bidirectional Scattering Surface Reflectance Distribution Function (BSSRDF) $S(x_i, \omega_i, x_o, \omega_o)$, an eight dimensional function that relates the incident illumination at a surface point x_i in a given direction ω_i to the outgoing illumination at a surface point x_o in direction ω_o.

Often, the spatial and directional terms of the BSSRDF are assumed to be independent [10]. While this assumption greatly improves rendering performance, makes acquisition easier, and works for a large number of materials, it is easy to find examples of materials where it would fail. Consider the reflectance of a material made from layers of glass or plastic. The outgoing illumination surface and angular distribution depend on the incident angle. This example appears in everyday household objects such as a roll of adhesive tape shown on Figure 1.

It is true that a modern ray tracer can render such a system by physically modeling the entire three-dimensional geometry [2]. However, while modeling the full geometry may be possible for simple examples with structures on a viable scale, it becomes extremely difficult for complex systems with microscopic structures. Worse still, acquiring the geometry from a physical object at a scale that would produce subsurface scattering could require advanced and expensive techniques such as Optical Coherence Tomography (OCT) [3] or Computerized Tomography (CT) [16].

Many of such materials, though, are homogeneous. That is, the object is spatially uniform and does not have any spatially varying texture, but the subsurface scattering depends on the incident and outgoing angles as well as the distance traveled on the surface. Past work has shown that the general case can be approximated by linear combination of homogeneous BSSRDFs [15].

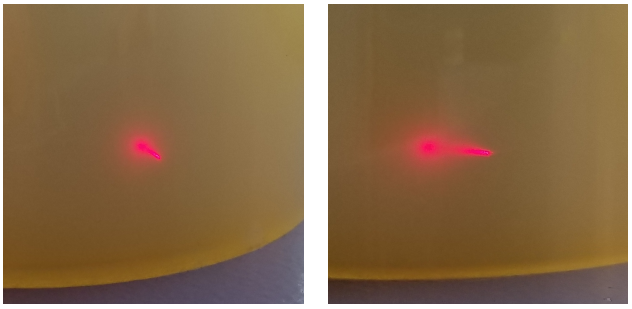

Figure 1. *A photograph showing a real world material, a roll of shipping tape, whose spatial scattering pattern depends on incident angle. In each image a handheld laser is focused on a point on the surface. Left image: the laser is incident in an approximately normal direction. The laser on the right is incident at a sharp angle.*

In this paper, we present a new method for acquiring subsurface scattering from homogeneous anisotropic materials. Our contributions include a novel acquisition system that is able to acquire (anisotropic) subsurface scattering; a demonstration of a coaxial acquisition system utilizing standard components and a new way of exploring material reflectance properties including subsurface scattering (Figure 10).

Subsurface Scattering Acquisition

In this section, we give a partial review of existing subsurface scattering acquisition systems and describe a working principle of the proposed device. For a more in-depth review of related work, we refer the reader to recent course notes on the topic [6].

BSSRDFs

The Bidirectional Scattering Surface Reflectance Distribution Function (BSSRDF) is a general description of light reflected at a surface when temporal, florescent, and nonlinear effects need not be taken into account. The BSSRDF is an 8-dimensional function and the general case of a BSSRDF can be approximated by the linear combination of homogeneous BSSRDFs [15]. Many materials exhibiting subsurface scattering are homogeneous. They are spatially uniform and do not have any spatially varying texture. In homogeneous BSSRDF the incident illumination location is irrelevant and the function can be parameterized as $S_H(\omega_i, r, \omega_o)$, where $r = \|x_i - x_o\|$ is the distance traveled on the surface.

A large amount of work has focused on acquiring the so called "diffusion" or "dipole" model, which assumes that the spatial scattering and scattering direction are independent from each other and the angle of incident illumination [10]. Furthermore,

the angular dependency is taken to be Fresnel terms:

$$S_H(\omega_i, r, \omega_o) = \frac{1}{\pi} F(\omega_i) R(r) F(\omega_o), \quad (1)$$

where $R(r)$ is a radial profile of subsurface scattering. With these simplifying assumptions in place, the BSSRDF can be obtained with a single HDR image [12].

Several dedicated devices have been designed to measure BSSRDFs. In [13], a specially designed water tank with an embedded light source is used to measure scattering properties of dilute substances. A few researchers have worked towards obtaining a more general BSSRDF. The DISCO system [5] used a laser to illuminate a 3D object at varying locations to capture the spatial distributions. However, it assumes that these spatial distributions are independent from both the incident and scattered angle distribution.

A family of acquisition devices, known as coaxial [7], utilize a beam splitter to combine the illumination and imaging channels. After the beam splitter, an optical system maps incoming rays to directions on the target surface. For most parts, coaxial devices are limited to reflectance at a point, that is a regular Bidirectional Reflectance Distribution Function (BRDF). However, a custom mirror front-end was used in [9] to obtain the BSSRDF.

In this paper, we describe a modification to the coaxial design that can extend the ability of many existing frontends designed to obtain BRDFs to obtain homogeneous BSSRDFs.

Light field imaging

In conventional camera, the rays forming an image B of an object A are fundamentally indistinguishable because they contribute to the same pixel. Installing a microlens array in front of the sensor (Figure 2) as proposed in [14] and having it focused to give an image of main lens aperture onto the sensor placed behind would overcome this limitation. The regular 2D image is turned into a 4D light field image where each macropixel (point B) corresponding to a single lenslet contains a sub-image of main lens aperture defining the distribution of rays forming that macropixel.

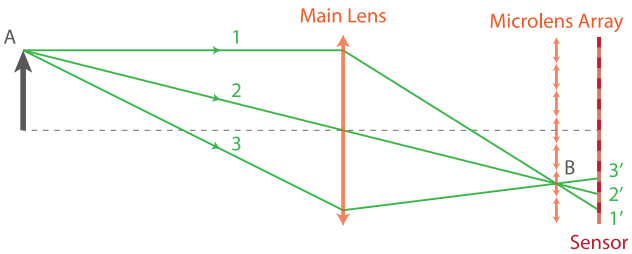

Figure 2. *An optical design of plenoptic camera. Unlike in conventional camera, the rays 1, 2 and 3 forming the image B of point A are distinguishable in plenoptic camera because of microlens array installed on top of the sensor.*

Lytro Illum is an example of a commercial light field camera of this design. However, it is not suitable for measuring BSSRDFs due to different design goals. One would end up building a low gain microscope similar to [11] trying to adapt it for BSSRDF acquisition. It is more important for BSSRDFs acquisition to have a high angular resolution rather than a high spatial resolution to capture specular effects. Also, the requirement of covering a significant portion of the hemisphere makes it impractical to use off-the-shelf lens assemblies.

BSSRDF acquisition using light field imaging

Consider a setup shown on Figure 3. When the incident illumination at a surface point x_i in a given direction ω_i is fixed, BSSRDF defines a light field $L(x_o, \omega_o)$ emanating from the surface of the material. Therefore, it is possible to measure a full BSSRDF by capturing the light field emitted by materials under different illumination conditions. We combine a light field imaging setup with illumination system by placing a beam splitter between the main lens and a multilens array.

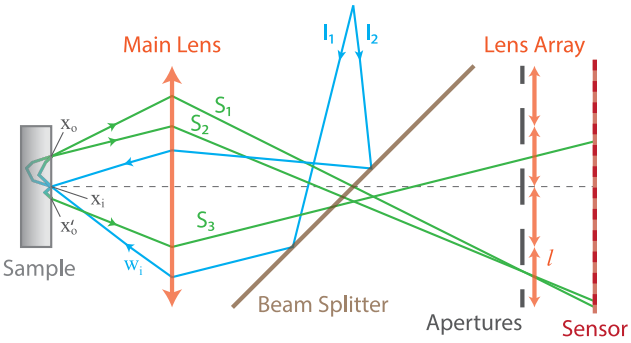

Figure 3. *Working principle. Incident rays are shown in blue and scattered rays are green. A central point x_i is illuminated by ray I_1 in a given direction ω_i. The scattered light exits the material surface at different location x_o due to the subsurface scattering. This location corresponds to a lenslet l in the array which gives an image of angular distribution of scattered light exiting at location x_o. Light exiting at different location x'_o contributes to the image of different lenslet (see ray S_3).*

A projector based illumination system is able to illuminate a point on a material's surface with an arbitrary angular distribution. Only one point x_i can be illuminated which does not limit the BSSRDF acquisition for homogeneous materials. Similar to a plenoptic camera, spatial resolution is defined by the number of lenslets in a lens array and the angular resolution is defined by the sensor resolution under each lenslet. We trade spatial resolution in favor of higher angular resolution for BSSRDF acquisition by using a lens array that has larger lenslets than a microlens array.

Matching the apertures

Our setup is based on the design of a handheld plenoptic camera presented in [14]. Therefore, it is essential to match the apertures of the main lens and multilens array to maximize the utilized sensor area while avoiding overlaps between images given by neighboring lenslets. Note that the reference design does not require any apertures being placed in front of the multilens array.

The distance between the main lens and multilens array defines the size of the sample area that is being scanned as shown by the purple extreme rays on Figure 4. The smaller the distance between the lens or, alternatively, the larger the multilens array and sensor size, the bigger the scanned area. Because many materials can exhibit subsurface scattering up to several millimeters from the illumination point, we also need to optimize the design to increase the scanned area.

Separation of spatial and angular components

Unlike the reference light field camera design, we need to place a small aperture in front of each lenslet for BSSRDF acqui-

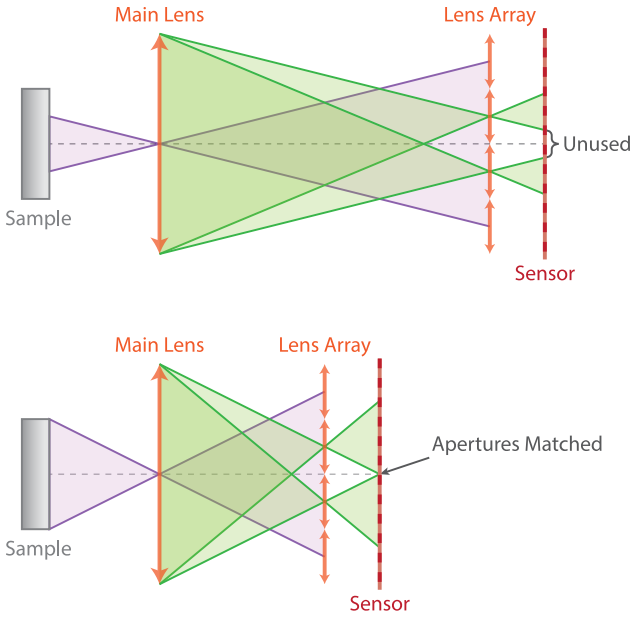

Figure 4. *Matching the apertures between main lens and multilens array increases the angular resolution of the system by maximizing the utilized sensor area. The scanned surface area of the sample increases as well.*

sition. As shown on Figure 5, the rays emanated at similar angles from the close points on a sample's surface may contribute to the same pixel on the sensor. This puts a principal limitation on the angular resolution of the acquired BSSRDF.

An aperture array placed in front of the multilens array is needed to separate the angular and spatial effects. The light contributing to the image of each lenslet is now limited to a smaller central part of the initial *bin* on the sample's surface corresponding to that lenslet. Another benefit of placing the aperture array is that it eliminates the cross-talk between the neighbor lenslets in the array which is inevitable due to the distortions caused by the strength of the main lens needed for better angular coverage. As an alternative to an aperture array, one could use the multilens array with smaller dimensions of the lenslets (smaller bins). However, smaller lenslets cover a smaller number of pixels on the sensor, decreasing the angular resolution.

Hardware Prototype

The BSSRDF acquisition prototype (Figure 6) consists of a projector, camera, light trap, beam splitter and main lens assembly (also referred to as objective lens). An up to scale schematic is shown on Figure 7. Starting from the projector, light travels through our system, being reflected off the beam splitter, traveling through the lens assembly, incidenting on the sample, returning back through the lens assembly and beam splitter, and finally being captured by the light field camera.

Our prototype is capable of measuring subsurface scattering up to 3 mm away from the illumination point with an angular resolution less than one degree. Although we cover a rather small part of the hemisphere (up to 30 degrees away from vertical versus, for example, 60 degrees in [8]), high angular resolution makes it possible to capture highly specular effects.

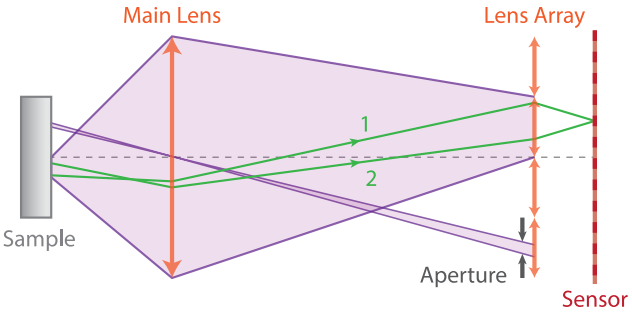

Figure 5. *Each lenslet in the array is collecting all the light coming from a corresponding bin on the sample's surface. This puts a principal limitation on the angular resolution of acquired BSSRDF because rays 1 and 2 coming from different locations at different angles may hit the same pixel and get confused. Placing a small aperture in front of the lenslet will limit the incoming light to the center of the bin only, separating in this way the angular and spatial effects in the scattered light field.*

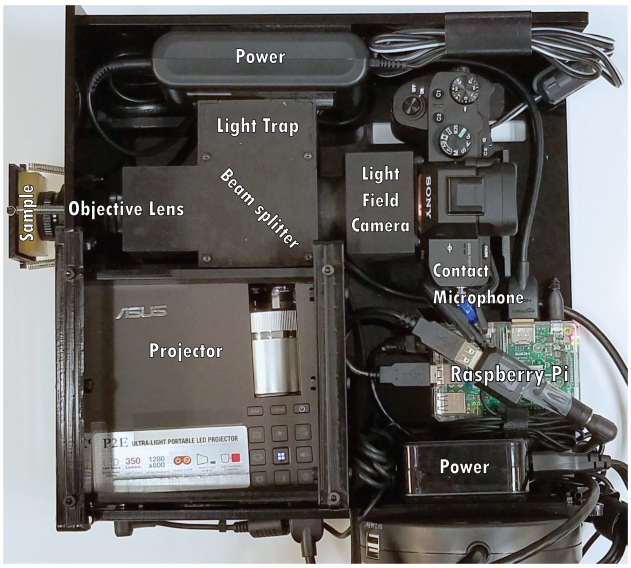

Figure 6. *A photo of BSSRDF acquisition prototype. The device is powered by Raspberry Pi, has a portable form-factor and capable of measuring up to 3 mm of subsurface scattering with high angular and spatial resolution.*

Design considerations

We place a small (1 mm) aperture directly in front of the projector lens so that rays forming the image of a single pixel at a 15 cm projecting distance have a divergence of less than 0.4 degrees (for reference, sunlight has a divergence of ≈0.5 degrees). Additionally, the illumination spot size is less than 200 μm (including distortions) because the objective lens are focused to give a sharp image of the projector aperture onto the sample. While this setup provides a high precision illumination and also the possibility to illuminate the sample with an arbitrary angular pattern, a modification of the projector lens was required (see Figure 8).

Having an objective lens with small f-number is necessary for better angular coverage but it induces a lot of distortions. Therefore, we are using an assembly of three achromatic lens as objective lens. Because objective lens are shared and can be focused at one distance at a time, the camera and projector apertures must both be located at the same distance from the objective lens.

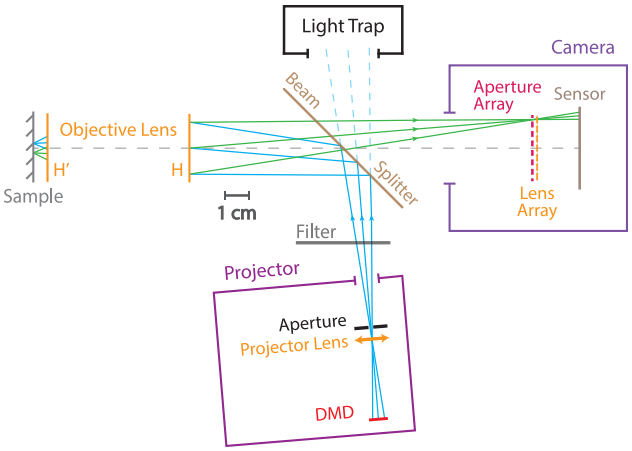

Figure 7. *An up to scale schematic of BSSRDF acquisition prototype. A point on a sample is illuminated by projecting a high resolution image onto objective lens. The scattered light is then captured by a light field camera complemented with an aperture array to separate angular and spatial components of BSSRDF. The light trap absorbs the projected light passing through the beam splitter to minimize the amount of back-reflection.*

At the same time, the camera (lens array) needs to be focused to give a sharp image of the H plane of the objective lens (see Figure 7) onto the sensor. The intensity of scattered light varies greatly for subsurface scattering and specular effects, requiring a High Dynamic Range (HDR) image capture.

Construction

The prototype was assembled from off-the-shelf components and 3D printed/laser cut parts with a total cost of around 3000 U.S. dollars. The camera is about half the total cost. The device has a portable form-factor and can be operated under normal illumination conditions due to its closed optical path. Scanning of non-flat surfaces is also possible, provided that the curvature is small compared to scanning area.

We use a Digital Micromirror Device (DMD) based projector model ASUS P2E with resolution of 1280x800 pixels and modified lens (Figure 8, left). DMD based projectors do not suffer from color bleeding as in [8] and have better contrast. Because each pixel is a fast-flipping micromirror and colors are time-multiplexed, the exposure times used have to be multiples of one over the refresh rate of the projector.

To maximize the scanned area, we utilize a full-frame Sony Alpha 7 II camera and a pair of 8x7 lens arrays with 4x3 mm individual lenslets (Figure 8, right). Unfortunately, the camera API does not provide a way to monitor when exposure is active, so we use a contact microphone (see Figure 6) to detect the shutter sound for synchronization of camera with projector.

The objective lens assembly has ≈8 times magnification, sample-side aperture of f/0.8 and a camera-side clear aperture of 22 mm. Coating of the lens is also important to mitigate back-reflections which are a significant source of background noise. The beam splitter with high transmission rate (75%) and coated second surface (to eliminate ghosts) is chosen for this purpose too. To minimize the amount of back-scattered light from the projector, a light trap was designed similar to an anechoic chamber and placed out of focus of the camera. All parts are painted black.

Figure 8. *Projector lens (left) have been modified to obtain small, closely focused image and to include a small aperture. A full-frame camera (right) has a custom lens array system installed comprising of a pair of lens arrays (to decrease the focal length) and apertures array is between.*

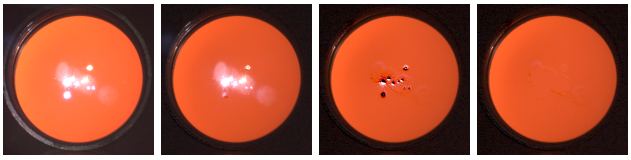

Figure 9. *Processing stages for a selected lenslet of HDR image captured for toothbrush case (Figure 10). Left to right: original image, blank frame subtracted only, blank and dark (with it's blank) frames subtracted, clean image with spurious pixel masked out.*

Calibration

We calibrate our prototype in three stages. First, we calibrate the camera sensor using a macbeth color chart. Afterwards, we jointly calibrate the camera and projector using a known light field. Finally, we improve the quality of acquired images by removing back-reflections (Figure 9).

We use RAW data capture and do all the postprocessing ourselves. The white balance of the projector is measured by capturing a spectrally neutral target placed out of focus of the objective lens, and remains constant for all captures. The response curve of the sensor is also experimentally measured similar to [1] and the resulting gamma value is 1.0077. Finally, we acquire several images at different exposures and combine them into a single HDR image.

The optical tract of the system has both illumination and imaging paths which can be calibrated separately. One way to calibrate the plenoptic camera is to take an image of a known light field. We use a simple circular pattern printed on large format and placed far from the objective lens. The projector can be calibrated by projecting the same pattern and adjusting the parameters so that it matches the printed one (the process needs to be performed in a dark room).

In addition to the projected pattern, there is a parasitic light illuminating the sample as well as reflecting back from the objective lens. The clean image of illumination pattern scattered by the sample can be obtained from:

$$clean = (pattern - blank) - (dark\_pattern - dark\_blank) \quad (2)$$

where $pattern$ and $blank$ are the images captured when the actual and blank (parasitic light only) patterns are projected with the sample being installed. $dark\_pattern$ and $dark\_blank$ are the corresponding images with the sample being removed (light is being projected into the empty space of a dark room). Figure 9 shows how image quality improves as Equation 2 is being computed.

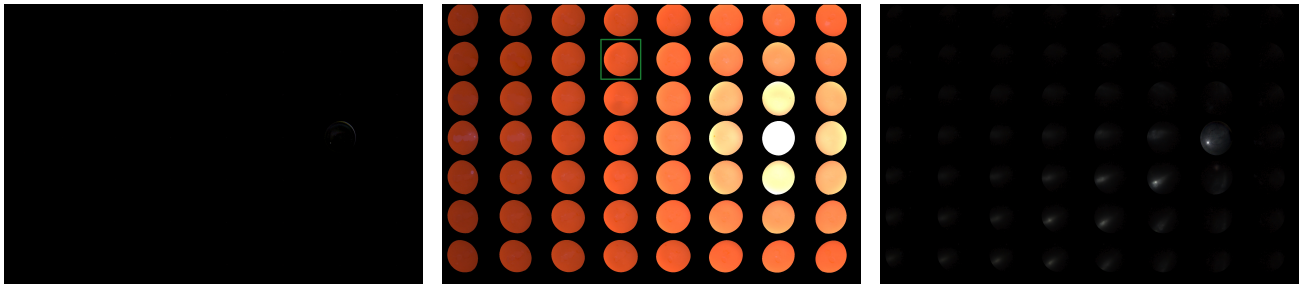

Figure 10. *An example of an HDR image for each of the three materials scanned to validate the device. Mirror (left) has no subsurface scattering, so all the reflected light is located in a primary lenslet. Toothbrush case (middle) exhibits isotropic subsurface scattering, thus, its lenslet are lit uniformly. Shipping tape (right) is highly anisotropic and one can see that it is scattering light mostly along the direction of incident light. Mirror and tape examples are given for $\theta = 20^\circ$ and $\theta = 30^\circ$ incident illumination. Toothbrush case is illuminated at normal angle. Mirror image was linearly mapped while toothbrush case and tape examples are $Gamma = 2.2$ mapped for better dynamic range representation. All images have pixels with signal to noise ratio less than two masked out after applying a Gaussian filter to suppress noise. The highlighted lenslet on middle image is the one used for Figure 9.*

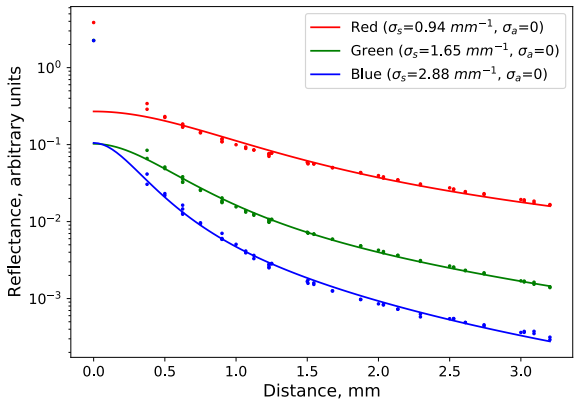

Figure 11. *A dipole model fitted to the measurements of diffuse light scattering in a plastic toothbrush case. Note that dipole model describes multiple (2 or more) scattering only. We cannot take single scattering into account because the first sample is already 0.5 mm away from the illumination point.*

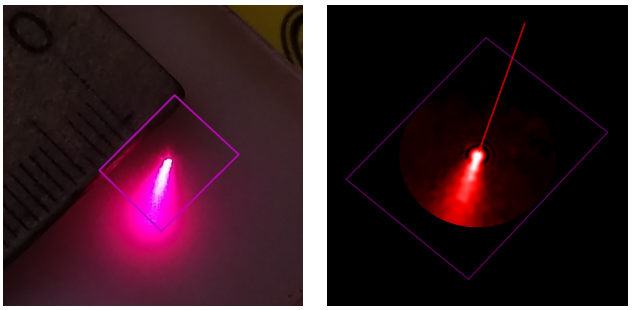

Figure 12. *A photo of shipping tape illuminated by laser beam at 20 degrees angle (left) and rendering of the same (no ambient light) setup based on measurements taken with our device (right). The rendering is done in red wavelength only and black-red-white colormap with $Gamma = 2.2$ mapping is used to match as close as possible the image processing done by the camera. The pink rectangle covers the same area on both images and the incident laser beam is denoted by the red arrow. A small amount of ambient light is provided to make the context of the photograph easier to see but might lead to a small color difference. Note that the ringing artifacts around illumination point are due to the RBF interpolation that might produces negative values.*

Results

We scan three different materials and show the samples of captured data on Figure 10. The acquisition time for 1008 points spaced uniformly over the covered part of the hemisphere is 1.4 hours in synchronous single-shot mode and can be as little as 6 min when using the burst mode of the camera (when the projector is synchronized by the shutter sound). The lenslet corresponding to the illumination point (referred to as primary) is the middle one in the second column from the right.

A mirror has no subsurface scattering and its BSSRDF is a delta function. It is used to determine the angular accuracy and resolution of the device which are equal to 0.75 arc degrees and 6.5 pixels correspondingly. The resolution value is used to choose an appropriate kernel size for sampling during rendering.

The material of the plastic toothbrush case exhibits diffuse subsurface scattering and we use it for quantitative validation of the device. Diffuse subsurface scattering can be described by the dipole model [10]. The radial profile of subsurface scattering in this model (Equation 1) depends on four parameters:

$$R(r) = R(r, \sigma_s, \sigma_a, \eta, \alpha) \tag{3}$$

We use an empirical value $\eta = 1.3$ and the remaining parameters (scattering, absorption coefficients and albedo) are subject to optimization. The optimization problem is under-constrained (constraint on total reflectance is missing), so we can only compare the functional behavior of the fitted model and it is in good agreement with measured data (see Figure 11).

The shipping tape is used as an example of a real-world layered material with anisotropic subsurface scattering. Figure 10 shows a sample scattered light field for illumination at 30 degrees vertical angle. It is apparent that it scatters light predominantly in the direction of illumination explaining the scattering pattern shown on Figure 1. Its diffuse component of yellowish color is not visible because it is very dim and is below the noise level for a given illumination.

To further validate the correctness of captured data we provide a qualitative comparison of a real-world photo of shipping tape under incident laser beam illumination with data-driven rendering of the same setup (Figure 12). We use a flat disk sampling kernel of radius 5 pixels with smooth edges and note that data-driven rendering will inevitably contain artifacts compared to model-driven renderings. We refer the reader to supplementary material for more details on how the rendering is being done.

Conclusion

This paper provides a tool for exploration of subsurface scattering in materials as is, by directly measuring it without any simplifying assumptions. We present an easily reproducible and low cost BSSRDF acquisition system built from off-the-shelf optical components and 3D printed/laser cut parts. Our prototype is able to measure subsurface scattering in homogeneous materials up to 3 mm away from the illumination point with angular coverage of up to 30 degrees from vertical. We validated our device by scanning materials with known properties. A mirror is used to measure angular accuracy and resolution. A plastic toothbrush case exhibiting diffuse subsurface scattering can be described by a dipole model which is in good agreement with measurements obtained by our device. Finally, we are able to reproduce the real-world appearance of a layered material with an anisotropic subsurface scattering such as shipping tape.

The main limitations of our setup arise from the requirement to have a high coverage of the hemisphere and a large scanned area at the same time. Whereas the latter linearly depends on the parameters of the setup such as focal lengths and dimensions, the former is bounded by the arc-tangent of the ratio between the main lens diameter and its focal length. Our goal was to build the system from off-the-shelf components. Therefore, it limits greatly the choice of parameters and many of them are not optimal. We believe that there is still room for improvement with existing components and we foresee a great improvement to acquisition speed by employing the ability of our setup to illuminate the sample with arbitrary angular patterns and using basis functions as in [4].

References

[1] Paul E. Debevec and Jitendra Malik. Recovering high dynamic range radiance maps from photographs. In *Proceedings of the 24th Annual Conference on Computer Graphics and Interactive Techniques*, SIGGRAPH '97, pages 369–378, New York, NY, USA, 1997. ACM Press/Addison-Wesley Publishing Co.

[2] Craig Donner, Tim Weyrich, Eugene d'Eon, Ravi Ramamoorthi, and Szymon Rusinkiewicz. A layered, heterogeneous reflectance model for acquiring and rendering human skin. In *ACM SIGGRAPH Asia 2008 Papers*, SIGGRAPH Asia '08, pages 140:1–140:12, New York, NY, USA, 2008. ACM.

[3] Alexander Doronin and Igor Meglinski. Imaging of subcutaneous microcirculation vascular network by double correlation optical coherence tomography. *Laser & Photonics Reviews*, 7(5):797–800, 2013.

[4] A. Ghosh, S. Achutha, W. Heidrich, and M. O'Toole. Brdf acquisition with basis illumination. In *2007 IEEE 11th International Conference on Computer Vision*, pages 1–8, Oct 2007.

[5] Michael Goesele, Hendrik Lensch, Jochen Lang, Christian Fuchs, and Hans-Peter Seidel. Disco: acquisition of translucent objects. In *ACM Transactions on Graphics (TOG)*, volume 23, pages 835–844. ACM, 2004.

[6] Giuseppe Claudio Guarnera, Abhijeet Ghosh, Ian Hall, Mashhuda Glencross, and Dar'ya Guarnera. Material capture and representation with applications in virtual reality. In *ACM SIGGRAPH 2017 Courses*, SIGGRAPH '17, pages 6:1–6:72, New York, NY, USA, 2017. ACM.

[7] Michael Holroyd, Jason Lawrence, and Todd Zickler. A coaxial optical scanner for synchronous acquisition of 3d geometry and surface reflectance. In *ACM Transactions on Graphics (TOG)*, volume 29, page 99. ACM, 2010.

[8] Chika Inoshita, Seiichi Tagawa, Md Abdul Mannan, Yasuhiro Mukaigawa, and Yasushi Yagi. Full-dimensional sampling and analysis of bssrdf. 5:119–123, 07 2013.

[9] Chika Inoshita, Seiichi Tagawa, Md Abdul Mannan, Yasuhiro Mukaigawa, and Yasushi Yagi. Full-dimensional sampling and analysis of bssrdf. *Information and Media Technologies*, 8(4):1105–1109, 2013.

[10] Henrik Wann Jensen, Stephen R. Marschner, Marc Levoy, and Pat Hanrahan. A practical model for subsurface light transport. In *Proceedings of the 28th Annual Conference on Computer Graphics and Interactive Techniques*, SIGGRAPH '01, pages 511–518, New York, NY, USA, 2001. ACM.

[11] Marc Levoy, Ren Ng, Andrew Adams, Matthew Footer, and Mark Horowitz. Light field microscopy. In *ACM SIGGRAPH 2006 Papers*, SIGGRAPH '06, pages 924–934, New York, NY, USA, 2006. ACM.

[12] Adolfo Munoz, Jose I Echevarria, Francisco J Seron, Jorge Lopez-Moreno, Mashhuda Glencross, and Diego Gutierrez. Bssrdf estimation from single images. In *Computer Graphics Forum*, volume 30, pages 455–464. Wiley Online Library, 2011.

[13] Srinivasa G Narasimhan, Mohit Gupta, Craig Donner, Ravi Ramamoorthi, Shree K Nayar, and Henrik Wann Jensen. Acquiring scattering properties of participating media by dilution. In *ACM Transactions on Graphics (TOG)*, volume 25, pages 1003–1012. ACM, 2006.

[14] Ren Ng, Marc Levoy, Mathieu Brédif, Gene Duval, Mark Horowitz, and Pat Hanrahan. Light field photography with a hand-held plenoptic camera. *Computer Science Technical Report CSTR*, 2(11):1–11, 2005.

[15] Pieter Peers, Karl vom Berge, Wojciech Matusik, Ravi Ramamoorthi, Jason Lawrence, Szymon Rusinkiewicz, and Philip Dutré. A compact factored representation of heterogeneous subsurface scattering. In *ACM SIGGRAPH 2006 Papers*, SIGGRAPH '06, pages 746–753, New York, NY, USA, 2006. ACM.

[16] Shuang Zhao, Wenzel Jakob, Steve Marschner, and Kavita Bala. Building volumetric appearance models of fabric using micro ct imaging. In *ACM SIGGRAPH 2011 Papers*, SIGGRAPH '11, pages 44:1–44:10, New York, NY, USA, 2011. ACM.

Author Biography

Yurii Piadyk received his MS in physics from the Taras Shevchenko National University of Kyiv (2016) and is pursuing PhD in computer science from New York University. He is working as research assistant in Visualization and Data Analytics Lab (ViDA) and his work is focused on imaging for sports analytics and computer graphics.

Yitzchak Lockerman received his Masters (2014) and PhD (2016) degrees in computer science from the Yale University. Since then he has worked as postdoctoral researcher at NYU Tandon School of Engineering. His primary research focuses on texture modeling, material modeling, data acquisition, and data analysis.

Claudio Silva received a BS in mathematics from the Federal University of Ceará (Brazil) in 1990, and a PhD in computer science from State University of New York at Stony Brook in 1996. He is a professor of computer science and engineering and data science at New York University. His primary research interests are in visualization, geometric computing, data science, sports analytics, and urban computing.

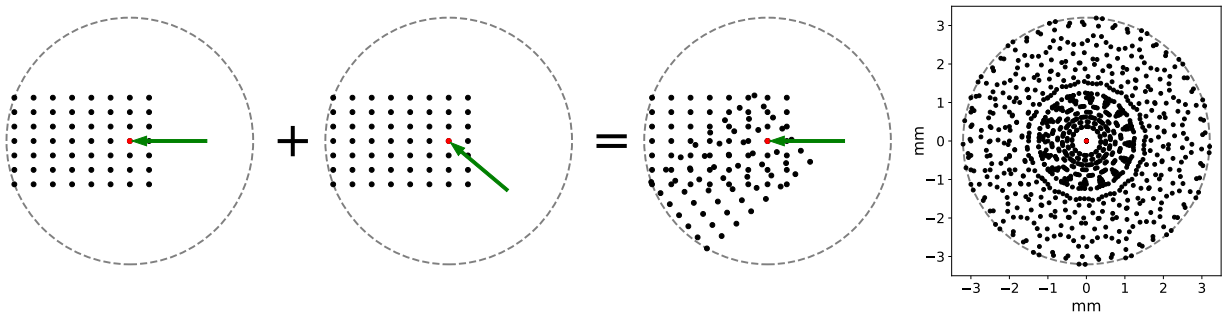

Figure 13. *Homogeneous materials that are also invariant to rotation with respect to the normal can be scanned with increased spatial resolution. Spatial samples obtained from single images when illuminating material at different ϕ but same θ angles ($\phi = 0^\circ$ for the first and -40° for the second image) can be combined as shown on the third image. 16 different illumination directions are enough to significantly increase the density of spatial samples (right).*

Appendix: Rotational Invariance

A shipping tape (Figure 1) is an example of layered homogeneous material with anisotropic subsurface scattering. By definition, homogeneous materials are invariant with respect to translation. In this example, it is also invariant with respect to rotation along the normal. That is, the scattering pattern does not depend on ϕ angle of incident illumination but on θ only. It means on practice that one can simply always measure the ϕ angle with respect to the projection of illumination direction onto the material surface (the green arrow on Figure 13).

A single image taken by the camera provides a grid of 8 x 7 *spatial samples* with one that is shown red on Figure 13 corresponding to the illumination point and referred to as primary. If the illumination point is not in the center, when illuminating at different ϕ angles one will be measuring scattered light on one side only with respect to the illumination point (first and second illustration on Figure 13).

The above properties allow spatial samples obtained at different illumination directions to be combined into a much denser grid (Figure 13, right). Because all spatial samples are located on circles around the illumination point, using the lens array with lenslets of uneven dimensions (rectangles instead of squares) is preferred as it yields more different radius values to sample at. Another benefit of such design compared to the primary lenslet being located in the center of the lens array is that the maximum distance away from illumination point where subsurface scattering can still be measured is increased by about 50% (3 mm instead of 2 in our case). This requires the projector's optical axis to be tilted with respect to the optical axis of camera/objective lens (see Figure 7).

For the rendering shown on Figure 12, we scan 24 uniformly spaced ϕ direction for $\theta = 20^\circ$ incident laser beam direction. An example of HDR image taken for $\phi = 30^\circ$ is shown on Figure 10 (right). After combining, spatial samples that are overlapping or are closer than $70\mu m$ to each other are averaged and replaced by a single sample. To further improve the rendering quality, a diffusion-like smoothing is performed on samples grid where the value of each sample is replaced by the average of its original value and the average of its neighbors (it conserves the total energy approximately). The result generally matches the real-world photo of the same setup but there are still some artifacts present due to the RBF interpolation that might produces negative values.

It should be emphasized that our device is capable of scanning materials that are not rotation invariant. The rotational invariance is only necessary to apply the technique described in this section. Non-rotationally invariant materials can be scanned directly but will not have an increased spatial resolution.